NEUROSCIENCE
RESEARCH ARTICLE

INTERNATIONAL BRAIN IBRO RESEARCH ORGANIZATION

P. Balaram et al. / Neuroscience xxx (2018) xxx–xxx

Synergistic Transcriptional Changes in AMPA and $GABA_A$ Receptor Genes Support Compensatory Plasticity Following Unilateral Hearing Loss

P. Balaram, [a,b†] **T. A. Hackett** [c] **and D. B. Polley** [a,b*]

[a] *Eaton-Peabody Laboratories, Massachusetts Eye and Ear Infirmary, Boston MA 02114, USA*

[b] *Dept. of Otolaryngology, Harvard Medical School, Boston MA 02114, USA*

[c] *Dept. of Hearing and Speech Sciences, Vanderbilt Bill Wilkerson Center for Otolaryngology and Communication Sciences, Vanderbilt University Medical Center, Nashville TN 37232 USA*

Abstract—Debilitating perceptual disorders including tinnitus, hyperacusis, phantom limb pain and visual release hallucinations may reflect aberrant patterns of neural activity in central sensory pathways following a loss of peripheral sensory input. Here, we explore short- and long-term changes in gene expression that may contribute to hyperexcitability following a sudden, profound loss of auditory input from one ear. We used fluorescence *in situ* hybridization to quantify mRNA levels for genes encoding AMPA and $GABA_A$ receptor subunits (*Gria2* and *Gabra1*, respectively) in single neurons from the inferior colliculus (IC) and auditory cortex (ACtx). Thirty days after unilateral hearing loss, *Gria2* levels were significantly increased while *Gabra1* levels were significantly decreased. Transcriptional rebalancing was more pronounced in ACtx than IC and bore no obvious relationship to the degree of hearing loss. By contrast to the opposing, synergistic shifts in *Gria2* and *Gabra1* observed 30 days after hearing loss, we found that transcription levels for both genes were equivalently reduced after 5 days of hearing loss, producing no net change in the excitatory/inhibitory transcriptional balance. Opposing transcriptional shifts in AMPA and GABA receptor genes that emerge several weeks after a peripheral insult could promote both sensitization and disinhibition to support a homeostatic recovery of neural activity following auditory deprivation. Imprecise transcriptional changes could also drive the system toward perceptual hypersensitivity, degraded temporal processing and the irrepressible perception of non-existent environmental stimuli, a trio of perceptual impairments that often accompany chronic sensory deprivation.

This article is part of a Special Issue entitled: [SI: Tinnitus Hyperacusis].

Key words: tinnitus, hyperacusis, hearing loss, auditory neuropathy, homeostatic plasticity, gene transcription.

INTRODUCTION

An acute loss of peripheral sensory input in adulthood triggers widespread compensatory changes in the central visual, auditory, and somatosensory pathways (Merzenich et al., 1983; Robertson and Irvine, 1989; Kaas et al., 1990; Jones and Pons, 1998; Wang et al., 2002; Kamke et al., 2003; Petrus et al., 2015; Humanes-Valera et al., 2017; Jaepel et al., 2017; Jiang et al., 2017; Asokan et al., 2018). For example, lesioning approximately 95% of cochlear nerve afferent synapses virtually eliminates sound-evoked responses in the auditory nerve, yet auditory responses recover nearly to baseline levels over a several week period in the auditory cortex (ACtx) (Chambers et al., 2016a; Resnik and Polley, 2017). Increased "central gain" in downstream areas of central auditory processing may support an adaptive recovery of sound detection thresholds despite widespread peripheral damage (Schuknecht and Woellner, 1953; Zeng, 2005; Lobarinas et al., 2013; Chambers et al., 2016a). The perceptual benefits of increased neural amplification are offset by a greater risk for debilitating perceptual consequences including hypersensitivity to moderately intense stimuli (e.g., hyperacusis) or the perceptual attribution of phantom stimuli to deafferented regions of the periphery (e.g., phantom limb pain, visual release hallucinations, or tinnitus) (Yang et al., 2011; Auerbach et al., 2014).

If pathologically over-powered "neural amplifiers" in sensory brain areas are at the root of these perceptual disorders, developing strategies to turn down their gain will require a detailed understanding of the biological mechanisms supporting neural amplification.

*Corresponding author.
E-mail address: daniel_polley@hms.harvard.edu (D. B. Polley).
† Present address: Allen Institute for Brain Science, 615 Westlake Ave, Seattle, WA 98109, USA.

Abbreviations: ABR, auditory brainstem response; ACtx, auditory cortex; DPOAE, distortion product otoacoustic emission; IC, inferior colliculus; STUD, short-term unilateral deafening.

https://doi.org/10.1016/j.neuroscience.2018.08.023
0306-4522/

Activity-dependent shifts in neural activity partly arise through number, subunit composition or cellular distribution of neurotransmitter receptors (O'Brien et al., 1998; Kilman et al., 2002; Marsden et al., 2007; Zhang et al., 2015). Dynamic shifts in postsynaptic receptor expression accompany normal auditory learning (Sun et al., 2005; Cai et al., 2010) and development (Kotak et al., 1998; Caicedo and Eybalin, 1999; Sanes and Kotak, 2011). Age-related hearing loss is accompanied by changes in GABA receptor distributions across the IC and ACtx (Gutiérrez et al., 1994; Milbrandt et al., 1994, 1997; Raza et al., 1994; Caspary et al., 1995, 2013; Yu et al., 2006), alongside changes in NMDA receptor distributions (Shim et al., 2012). Further, acute cochlear trauma leads to altered distributions of excitatory and inhibitory postsynaptic receptors in the brainstem (Suneja et al., 2000; Dong et al., 2009, 2010a), IC (Holt et al., 2005; Dong et al., 2010b), and ACtx (Wang et al., 2005).

In this report, we investigated changes in transcription levels for genes encoding subunits of excitatory and inhibitory neurotransmitter receptors following a sudden loss of auditory peripheral input in young adult animals. Prior reports in several different sensory systems have described reduced $GABA_A$ receptor expression following a loss of peripheral afferent input (Wong-Riley and Jacobs, 2002; Garraghty et al., 2006; Mowery et al., 2015), including the adult auditory system (Suneja et al., 2000; Dong et al., 2010b; Yang et al., 2011). Sensory neurons can also compensate for reduced activity levels through increased expression of glutamatergic AMPA receptors (Turrigiano et al., 1998; Suneja et al., 2000; Holt et al., 2005; Dong et al., 2010a; Teichert et al., 2017). We therefore chose to quantify mRNA levels of *Gria2*, which encodes the GluA2 subunit of AMPA receptors, and *Gabra1*, which encodes the α1 subunit of GABAA receptors, approximately one month following a near-complete loss of cochlear afferent neurons. Prior studies have reported that neurophysiological compensation for peripheral afferent lesions is more complete in the cortex than the midbrain (Qiu et al., 2000; Chambers et al., 2016a). Here we contrast the degree of transcriptional changes in *Gria2* and *Gabra1* mRNA levels between the IC and ACtx to determine whether hierarchical differences in central compensation are also found at the level of gene transcription. By taking advantage of novel fluorescence mRNA hybridization techniques that allow multi-channel single-molecule visualization in tissue sections, we quantified *Gria2* and *Gabra1* mRNA levels within single cells in each condition. Using this approach, we find opposing shifts in *Gria2* and *Gabra1* expression in the IC and ACtx after one month of near-complete cochlear denervation. Transcriptional shifts are proportionately larger in ACtx compared to the IC, which could underlie the more robust recovery of physiological responsiveness at the level of the cortex, when compared to the midbrain.

EXPERIMENTAL PROCEDURES

All procedures were approved by the Institutional Animal Care and Use Committee at the Massachusetts Eye and Ear Infirmary and followed the guidelines established by the National Institutes of Health for the care and use of laboratory animals. Seven male CBA/CaJ mice (Jackson Labs), aged 10–12 weeks, and six CamKII-tTA × tetO-GCaMP6s mice on a C57BL6 background of both sexes (Wekselblatt et al., 2016), aged 5–6 weeks, were used in this study.

Unilateral cochlear denervation with ouabain

CBA/CaJ mice were anesthetized with ketamine (120 mg/kg) and xylazine (12 mg/kg), with supplemental doses of ketamine (60 mg/kg) administered as needed. Core body temperature was maintained at 36.7 °C with a homeothermic heating pad. After numbing the left ear with a local anesthetic, a semicircular incision was made and the superficial fascia and muscle tissue were blunt retracted to expose the bulla. A small opening was made in the bulla with a 28.5-gauge needle to expose the round window niche. The exposed round window niche was then either filled with ouabain solution (1–2 μL, 1 mM in distilled water; $N = 4$) or with distilled water vehicle ($N = 3$) using a blunted needle. Ouabain or distilled water was reapplied 5–7 more times at 15-minute intervals, wicking the existing solution away before each new application. Distortion product otoacoustic emission (DPOAE) and auditory brainstem response (ABR) were measured following the sixth application, either to confirm normal DPOAE and ABR thresholds in vehicle-treated mice or elevated ABR thresholds with normal DPOAE in ouabain-treated mice. If ABR thresholds with 16-kHz tone pips (see below) were < 60 dB SPL after six ouabain applications, one or two more applications were performed until the ABR threshold was > 60 dB SPL without inducing any obvious shift in DPOAE threshold. The incision was closed, Bacitracin applied to the wound margin, and Buprenex (0.5 mg/kg) administered subcutaneously as an analgesic. Mice were transferred to a heated recovery chamber before returning to their home cage.

Unilateral cochlear deafening with sterile water

Short-term unilateral deafening (STUD) or a control procedure was performed on a separate cohort of transgenic mice ($N = 6$) on a C57BL6 background (CamKII-tTA × tetO-GCaMP6s); Jackson labs stock numbers 003010 and 024742, respectively). Mice were brought to a surgical plane of anesthesia using ketamine (120 mg/kg) and xylazine (12 mg/kg), with supplemental doses of ketamine (60 mg/kg) administered as needed. Before inducing STUD ($N = 3$ mice), DPOAEs and ABRs were first measured in the left ear to confirm normal cochlear function. The tympanic membrane and middle ear ossicles were then removed with fine forceps. A flexible canula was then attached to the exposed oval window and a 1–2 μL bolus of distilled water was flushed through the oval window opening. ABR and DPOAE were measured after every 2–4 flushes until the DPOAE was not measurable and the ABR threshold was > 60 dB SPL. The middle ear cavity was then packed with sterile cotton, the pinna

Please cite this article in press as: Balaram P et al. Synergistic Transcriptional Changes in AMPA and $GABA_A$ Receptor Genes Support Compensatory Plasticity Following Unilateral Hearing Loss. Neuroscience (2018), https://doi.org/10.1016/j.neuroscience.2018.08.023

incision was sutured closed and covered with Bacitracin. Buprenex (0.5 mg/kg) was administered subcutaneously before mice were transferred to a warmed recovery chamber. For the control procedure ($N = 3$), DPOAEs and ABRs were measured in the left ear, Buprenex (0.5 mg/kg) was subcutaneously administered, and animals were transferred to a heated chamber to recover as described above. Five days after control or STUD surgery, animals were anesthetized as described above and sterile cotton removed from the middle ear. DPOAE and ABR thresholds were measured in the left ear to confirm profound elevations in ABR and DPOAE thresholds in STUD mice and normal thresholds in control mice.

Cochlear function tests

ABR and DPOAEs were measured at a single frequency (16 kHz) during the cochlear denervation surgery and measured again at multiple frequencies just prior to processing of brain tissue (Fig. 1A). All measurements were performed under anesthesia with core body temperature maintained at 36.7 °C, as described above. ABR recordings were made with transdermal electrodes (Grass Technologies, Natus Medical Inc.) either arranged in the standard pinna to vertex montage (ouabain denervation) or a pinna-pinna horizontal montage (STUD) and focused on wave 1, which arises from the auditory nerve compound action potential (Melcher et al., 1996; Galbraith et al., 2006). Acoustic stimuli were generated with a 24-bit digital-to-analog converter (PXI-4461, National Instruments) and delivered using custom in-ear acoustic assemblies consisting of two miniature dynamic earphones (CUI CDMG15008-03A) and an electret condenser microphone (Knowles FG-23339-PO7) coupled to a probe tube. Sound levels were calibrated in the ear canal for each mouse prior to every recording session.

DPOAE stimuli were primary tones – 8, 11.3, 16, 22.6, and 32 kHz – presented in 5-dB steps from 20- to 80-dB SPL, with a frequency ratio of 1.2 and the f2 primary level 10 dB below the corresponding f1 level. We then calculated the sound pressure level at the 2f1–f2 DPOAE frequency as well as the acoustic noise floor. DPOAE threshold was defined as the lower of at least two continuous levels where the DPOAE was at least 5 dB above the acoustic noise floor. The ABR was elicited with tone pips (8, 16, and 32 kHz, 5-ms duration, with 0.5 ms raised cosine onset and offset ramps). Tones were presented in 5-dB steps from 20- to 80-dB SPL, repeated 512 times each. ABR threshold was defined at each frequency as the lowest sound level at which a repeatable waveform could be identified. Visual identification of the waveform was validated with a semi-automated algorithm that identifies peaks and troughs of putative ABR waves by first calculating the negative zero crossings of the first derivative of the recorded waveform. The algorithm eliminates spurious peaks by setting a threshold for negative zero crossing amplitude based on the noise floor, calculated from the standard deviation of the first 1 ms of the signal (Buran et al., 2010).

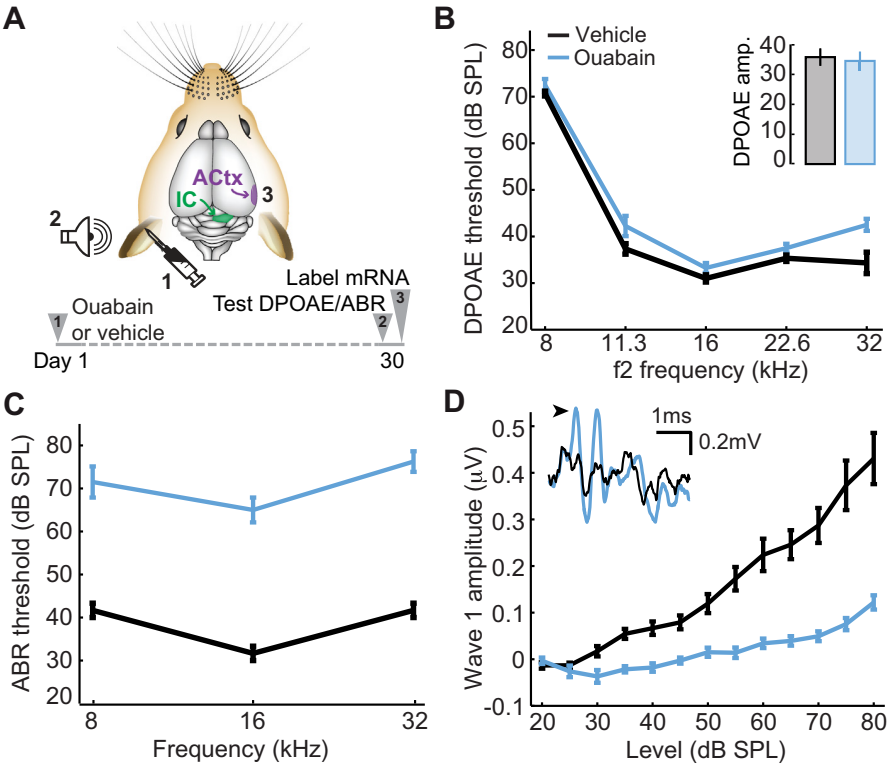

Fig. 1. Cochlear application of ouabain elevates ABR thresholds with minimal effects on DPOAEs. (A) A 1 mM Ouabain solution or distilled water (vehicle) was applied to the left ear of adult CBA/CaJ mice. Distortion product otoacoustic emissions (DPOAEs) and auditory brainstem responses (ABRs) were measured 30 days later, just before processing tissue from the contralateral inferior colliculus (IC) and auditory cortex (ACtx) for *in situ* hybridization. (B) DPOAE thresholds from ouabain- and vehicle-treated ears (blue and black, respectively). *Inset:* DPOAE emission amplitude at 60-dB SPL from the same ears. (C, D) ABR wave 1b thresholds presented at particular test frequencies (C) or wave 1b amplitude growth functions averaged across test frequencies (D). *Inset:* representative ABR waveforms from vehicle- and ouabain-treated ears evoked by 16-kHz tone pips at 70-dB SPL. Black arrowhead denotes wave 1b. All data are mean ± SEM.

Tissue acquisition and *in situ* hybridization

Unfixed brains were extracted and flash frozen in liquid nitrogen, and then embedded in OCT compound (TissueTek, VWR, Radnor, PA, USA). Embedded brains were secured in a −28 °C cryostat and cut into 10-μm coronal sections. Frozen sections were mounted on pre-chilled (−20 °C) Superfrost slides (Fisher Scientific, Waltham, MA, USA)

and stored at −80 °C. Fluorescence *in situ* hybridization for *Gria2* and *Gabra1* mRNA was performed on sections containing the ACtx or IC. Custom target probes were provided by Advanced Cell Diagnostics (ACD, Hayward, CA, USA), described previously (Hackett et al., 2015). Tissue permeabilization, mRNA hybridization and amplification, and fluorescent labeling were all performed using the RNAscope Multiplex Fluorescent Reagent Kit and HyBEZ oven (ACD, Hayward, CA, USA), according to the manufacturer's instructions for fresh-frozen brain tissue. Cell nuclei were counterstained with DAPI and sections were coverslipped with Vectashield (Vector Labs, Burlingame, CA, USA).

Image acquisition and analysis

For cochlear denervation experiments, three regions of interest (185 μm × 185 μm each) were imaged at three distinct caudal–rostral positions within the IC and ACtx. In the IC, all regions of interest were positioned centrally, in and around the central nucleus. In the ACtx, all regions of interest were positioned between layer 2/3 and layer 6 along a single cortical column. Anatomical landmarks were cross-referenced against our prior publications and published mouse brain atlases to ensure that all cortical ROIs fell inside the boundaries of ACtx (Hackett et al., 2011, 2015). Images were acquired with a Leica SP8 confocal microscope with a 63× 0.8NA immersion lens and two Leica HyD detectors. Image stacks were transferred to image-processing software (Amira, Visage Imaging) and projected in three dimensions. Perimeters of DAPI-labeled nuclei were identified by vectors of maximal intensity contrast between the DAPI-labeled region and image background, which consistently demarcated the outer edge of the labeled nucleus. Neighboring DAPI nuclei that were not segregated based on intensity contrast were manually separated using the Volume Edit tool in Amira. Large clusters of overlapping nuclei that could not be manually separated were excluded from analysis. Partial segments of DAPI nuclei, located along the image border or above and below the imaging planes, were also excluded from analysis. In the *Gria2* and *Gabra1* fluorophore channels, clusters of fluorescent pixels with a minimum diameter of 0.7–0.9 μm (4–5 pixels) were operationally classified as individual *Gria2* or *Gabra1* puncta. Single fluorescent clusters correspond to single mRNA copies, as previously described (Wang et al., 2012). Large pixel clusters that could be visually separated into individual puncta were also subdivided using the Volume Edit tool in Amira; clusters that exceeded 1.5 μm (8–10 pixels) and could not be visually separated were excluded from analysis. Identified *Gria2* and *Gabra1* puncta within 2.5–3.5 μm (15–20 pixels) of a DAPI-labeled perimeter were then counted and assigned to that cell using the Connected Components function in Amira. Transcript counts per cell were then exported to MATLAB (Mathworks).

Analysis of tissue from mice that underwent the STUD protocol focused only on ACtx, where three columnar regions across the caudal–rostral extent were imaged at 63× using a Leica DM5500B fluorescent microscope. Image stacks within each ROI were captured in 210 μm × 210 μm × 10 μm stacks with 0.5-μm z-plane spacing and stitched together using the Mosaic Merge tool in the Leica scope software (LASX). Tiled image stacks were then separated into individual fluorophore channels, and images were deconvolved in the Z dimension using the 3D deconvolution tool in LASX.

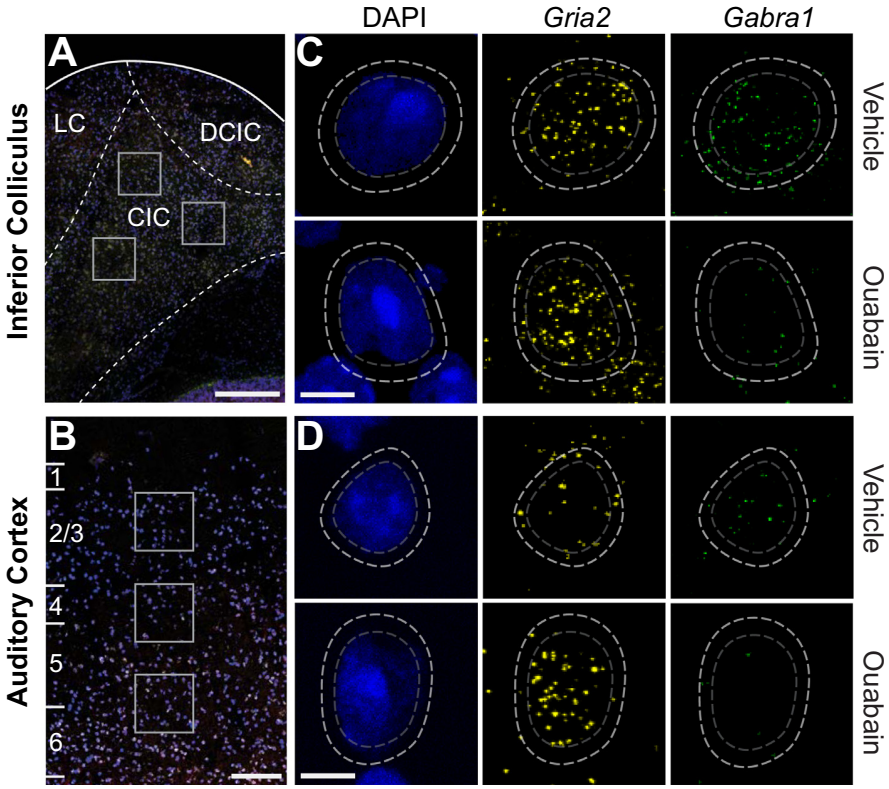

Fig. 2. Quantification of *Gria2* and *Gabra1* mRNA transcripts from single neurons in the inferior colliculus and auditory cortex. (A-B) Individual mRNA transcripts that encode subunits of AMPA and $GABA_A$ receptors (*Gria2* and *Gabra1*, respectively) were measured from regions of interest (white squares) in the IC (A) or ACtx (B) contralateral to the vehicle- or ouabain-treated ear. LC, DCIC and CIC represent the approximate boundaries of the Lateral Cortex, Dorsal Cortex of the IC and Central Nucleus of the IC, respectively. (C, D) Single cells were identified by DAPI labeling of the nuclear perimeter (dashed gray line). Representative *Gria2* (yellow) and *Gabra1* (green) mRNA levels in individual cells contralateral to vehicle- and ouabain-treated ears (top and bottom row, respectively). Fluorescently labeled individual mRNA transcripts are automatically identified within a fixed radius of each nucleus (dashed white line), counted, and then assigned to a given cell. Scale bars in *A* and *B* are 250 μm. Scale bars in *C* and *D* are 5 μm.

Please cite this article in press as: Balaram P et al. Synergistic Transcriptional Changes in AMPA and $GABA_A$ Receptor Genes Support Compensatory Plasticity Following Unilateral Hearing Loss. Neuroscience (2018), https://doi.org/10.1016/j.neuroscience.2018.08.023

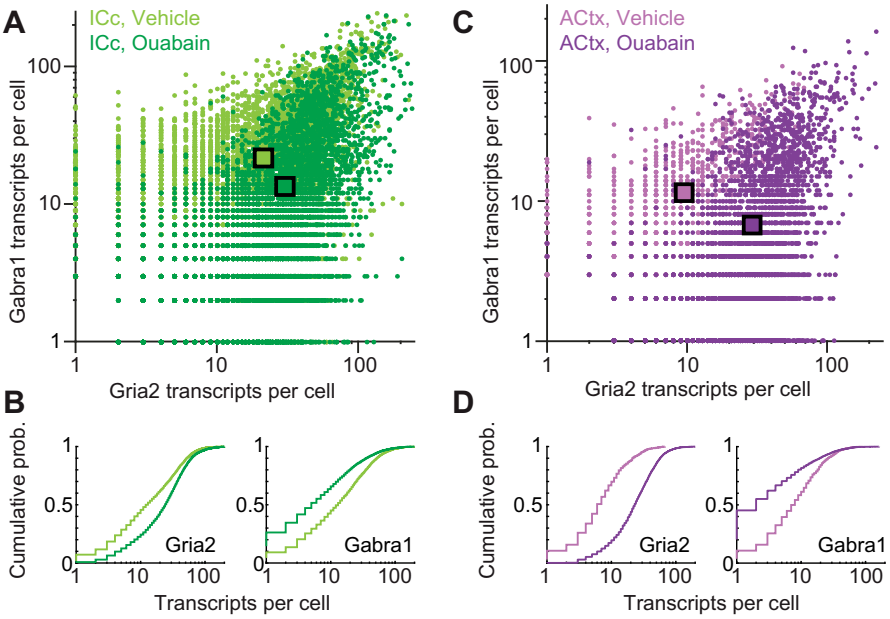

Fig. 3. Synergistic shifts in *Gria2* and *Gabra1* transcription following cochlear nerve damage. (A) Counts of *Gria2* and *Gabra1* transcripts in the IC contralateral to the vehicle- and ouabain-treated ears (light and dark green hue, respectively). Each point represents the number of transcripts for a given cell. Squares indicate means of the *Gria2* and *Gabra1* distributions for each treatment group. (B) Cumulative distributions of *Gria2* and *Gabra1* transcripts in vehicle- and ouabain-treated mice. (C, D) As per *A* and *B*, but for ACtx. Lighter and darker hues of purple represent cells contralateral to vehicle- and ouabain-treated ears, respectively.

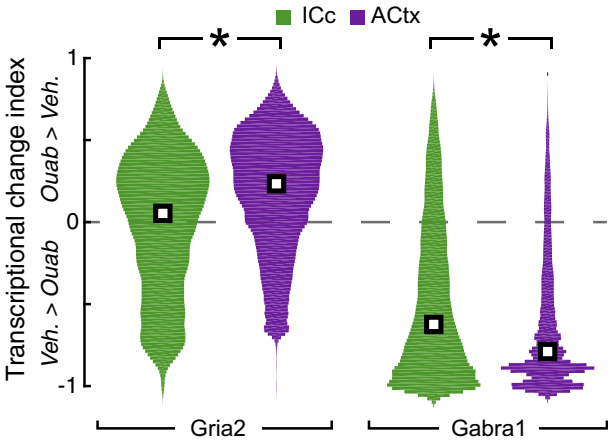

Fig. 4. Bi-directional changes in *Gria2* and *Gabra1* transcripts are more pronounced in ACtx than IC. Changes in *Gria2* and *Gabra1* transcript levels in each individual cell are expressed relative to the mean of the corresponding vehicle value according to the formula (# transcripts in single ouabain cell − mean transcript count from vehicle)/(# transcripts in single ouabain cell + mean transcript count from vehicle), where zero (dashed gray line) indicates no change relative to vehicle and positive and negative values represent increases or decreases relative to vehicle, respectively. White squares represent the median of each distribution. Veh. = vehicle. Asterisks indicate significant differences with a Wilcoxon Rank Sum test.

Images for each channel were collapsed across the z plane using the Maximum Intensity Projection tool in LASX, and then exported to MATLAB for further analysis. In MATLAB, images were converted to binary using a 50% threshold, which removed background fluorescence while preserving DAPI and mRNA label.

In DAPI images, individual cells were identified as isolated pixel clusters within 5–15 μm. In mRNA images, fluorescent puncta corresponding to individual mRNA transcripts were identified as isolated pixel clusters with diameters between 0.7 and 0.9 μm. Smaller clusters in all images were excluded from analysis. Larger clusters were further segmented by computing a distance transform within each cluster, generating a grayscale intensity image based on the distance transform, and applying a watershed algorithm to the grayscale image. Segmented regions were then identified as isolated cells or puncta based on the size requirements described above. Perimeters of identified DAPI nuclei were then radially dilated to delineate a putative cytosolic region for each cell, and isolated fluorescent puncta within this region in each fluorophore channel were counted and assigned to that cell. If dilated perimeters overlapped between cells, they were discarded from analysis. Cells with actual or dilated perimeters contacting the edge of the image were also discarded from analysis.

Statistics

Statistical analysis was performed in Matlab. The Lillefors test was used to determine whether any given sample was normally distributed. If data met the assumptions of parametric statistics, descriptive statistics were provided as means with standard errors and inferential statistics were performed with a mixed model ANOVA or unpaired *t*-tests. If data did not meet the assumptions of parametric statistics, descriptive statistics were provided as the median of a distribution and inferential statistics were performed with the Wilcoxon Rank Sum test.

RESULTS

Unilateral auditory nerve damage following application of ouabain to the cochlear round window

We selectively lesioned primary afferent neurons throughout the cochlear frequency map by applying ouabain to the cochlear round window. Ouabain is a Na^{2+}/K^{+} ATP-ase pump inhibitor that eliminates Type-I cochlear afferent neurons while inducing little damage to other sensory and non-sensory cell types in the inner ear (Lang et al., 2005; Yuan et al., 2013). In keeping with

Please cite this article in press as: Balaram P et al. Synergistic Transcriptional Changes in AMPA and $GABA_A$ Receptor Genes Support Compensatory Plasticity Following Unilateral Hearing Loss. Neuroscience (2018), https://doi.org/10.1016/j.neuroscience.2018.08.023

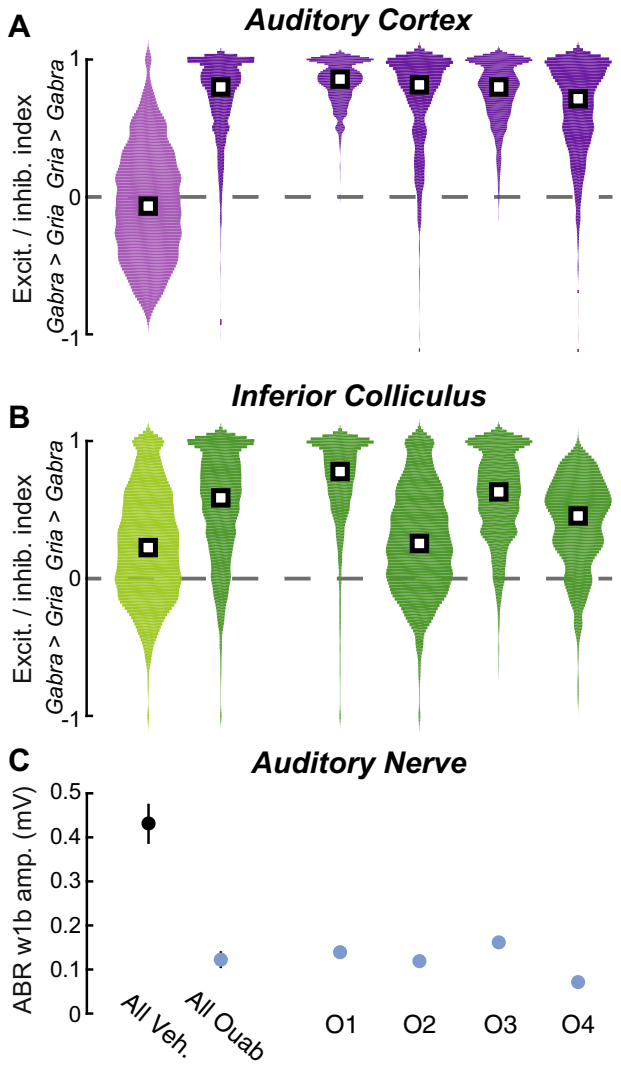

Fig. 5. Net transcriptional shifts show no obvious relationship to the extent of auditory nerve damage. (A, B) The distribution of excitation/inhibition (E/I) index values from all cells in ACtx (A) and IC (B), according to the formula (*Gria2* – *Gabra1*)/(*Gria2* + *Gabra1*), where zero (dashed gray line) indicates an equivalent number of excitatory (*Gria2*) and inhibitory (*Gabra1*) transcripts. E/I index values are pooled across all vehicle- and ouabain-treated mice (left) but are also shown separately for individual ouabain-treated mice (O1–4). (C) The mean amplitude of ABR wave1b at 80-dB SPL provides an index of auditory nerve damage in each ouabain-treated mouse (blue) as compared to vehicle-treated mice (black). Veh. = vehicle.

previous reports, we found that repeated application of ouabain at 1 mM concentration to the left ear was associated with a slight elevation of DPOAE threshold, a marker of pre-neural outer hair cell function (Fig. 1B, ANOVA, $F(1) = 12.2$, $p < 0.05$). Other than this modest threshold shift, hair cell function appeared normal, as DPOAE amplitudes measured at a suprathreshold level (60 dB SPL) were not different between ouabain- and vehicle-treated mice (Fig. 1B inset, unpaired *t*-test, $p = 0.77$).

By contrast, sound-evoked responses in the auditory nerve and brainstem were profoundly reduced due to the loss of primary afferent neurons that convey auditory signals from the inner ear to the brain. Thirty days following ouabain treatment, ABR thresholds were elevated by 30–40 dB across all test frequencies compared to vehicle-operated controls (Fig. 1C, ANOVA, $F(1) = 90.9$, $p < 0.0005$). Wave 1 of the ABR is generated by the synchronized compound action potentials of Type-I spiral ganglion neurons, where the amplitude of wave 1 is linearly related to the fraction of surviving synapses onto inner hair cells (Yuan et al., 2013; Chambers et al., 2016a). We found that the wave 1 sound level growth function was reduced by approximately 75% compared to vehicle-treated controls (Fig. 1D, ANOVA, $F(1) = 48.2$, $p < 0.0001$).

Opposing transcriptional shifts in AMPA and GABAA receptor subunit mRNA following auditory nerve damage

With a protocol in place to reduce afferent input from the auditory nerve, we next developed a strategy to quantify transcriptional changes in central auditory neurons that may support a compensatory plasticity. Given the long-recognized linkage between auditory deprivation and changes in GABA and AMPA receptors following auditory deprivation, we focused on quantifying changes in *Gria2* and *Gabra1* mRNA, which encode the GluA2 and α1 subunits of AMPA and $GABA_A$ receptors, respectively. We focused our analysis on the ACtx and IC contralateral to the denervated ear based on prior comparisons of physiological plasticity in these brain areas following selective cochlear afferent damage (Qiu et al., 2000; Chambers et al., 2016a).

We used fluorescent in situ hybridization followed by quantitative image analysis to label and count mRNA transcripts encoding AMPA and GABAA receptor subunits in single cells 30 days after ouabain ($N = 4$ mice) or vehicle ($N = 3$ mice) treatment. *Gria2* and *Gabra1* mRNA transcripts were labeled in the perinuclear area of individual neurons visualized in coronal sections through IC (Fig. 2A) and ACtx (Fig. 2B). As shown in these four representative neurons, we observed that *Gria2* and *Gabra1* transcript counts were approximately balanced in the IC and ACtx of vehicle-treated mice, but shifted in opposing directions 30 days after contralateral denervation, such that *Gria2* mRNA levels were increased while *Gabra1* levels were reduced (Fig. 2C-D, top vs bottom rows, respectively).

To quantify these changes, we implemented an automated analysis routine that *(i)* identified single-mRNA puncta, *(ii)* assigned them to a parent neuron, and *(iii)* counted them to quantify *Gria2* and *Gabra1* levels in individual neurons. Using this approach, we were able to quantify transcriptional markers for both excitatory and inhibitory neurotransmissions in thousands of single neurons in the IC (vehicle-treated, $n = 4125$ cells, ouabain-treated, $n = 6063$ cells) and ACtx (vehicle, $n = 2767$ cells, ouabain, $n = 4705$ cells). In the IC, we observed that contralateral cochlear denervation significantly increased *Gria2* levels compared to vehicle controls (30.54 ± 0.36 vs. 21.86 ± 0.29, mean ± SEM for ouabain and vehicle,

Please cite this article in press as: Balaram P et al. Synergistic Transcriptional Changes in AMPA and $GABA_A$ Receptor Genes Support Compensatory Plasticity Following Unilateral Hearing Loss. Neuroscience (2018), https://doi.org/10.1016/j.neuroscience.2018.08.023

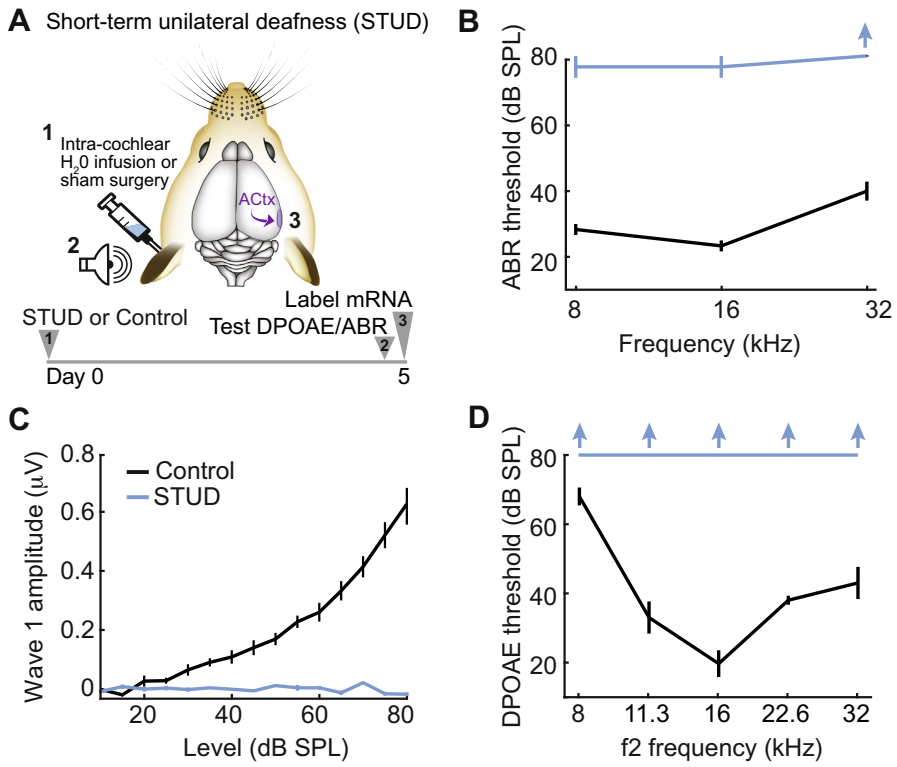

Fig. 6. Cochlear sterile water perfusion induces complete short-term unilateral deafness. (A) Schematic illustrates a protocol to induce short-term unilateral deafness (STUD) in the left ear through intracochlear perfusion of sterile water through the exposed cochlear oval window. Cochlear function and ACtx mRNA was measured 5 days after induction of STUD. (B–D) ABR threshold (B), wave 1 sound level growth functions (C) and DPOAE threshold (D) were measured in the left ear of control (black) or STUD (blue) mice. Upward arrows indicate no measurable response was detected at the highest sound level tested. All data are mean ± SEM.

respectively, unpaired *t*-test, $p < 1 \times 10^{-6}$). In the same cells, we observed that *Gabra1* transcripts were significantly reduced (13.34 ± 0.28 vs. 23.28 ± 0.32, mean ± SEM for ouabain and vehicle, respectively, unpaired *t*-test, $p < 1 \times 10^{-6}$, Fig. 3A-B). Opposing shifts in mRNA levels were also seen in ACtx, where cells expressed significantly higher levels of *Gria2* transcripts than controls (28.98 ± 0.34 vs. 9.52 ± 0.45, mean ± SEM for ouabain and vehicle, respectively, unpaired *t*-test, $p < 1 \times 10^{6}$) but significantly lower levels of *Gabra1* mRNA (6.73 ± 0.34 vs. 11.85 ± 0.53, mean ± SEM for ouabain and vehicle, respectively, unpaired *t*-test, $p < 1 \times 10^{6}$, Fig. 3C, D).

Hierarchical regulation of excitatory/inhibitory balance

Prior reports have described more complete compensatory plasticity in ACtx than IC following ouabain denervation. To extend this analysis to transcriptional changes we computed an asymmetry index bounded from −1 to +1, where a value of 0 is equivalent to the mean of the vehicle distribution for *Gria2* or *Gabra1* from the corresponding brain region (Fig. 4). We observed that *Gria2* elevation following contralateral denervation was more pronounced in the ACtx than in the IC (0.23 ± 0.51 vs. 0.05 ± 0.64, median ± IQR for ACtx and IC, respectively, Wilcoxon's rank sum, $p < 1 \times 10^{-6}$). We also found that reductions in *Gabra1* transcripts were significantly more pronounced in the ACtx compared to the IC (−0.79 ± 0.47 vs. −0.62 ± 0.76, median ± IQR for ACtx and IC, respectively, Wilcoxon's rank sum, $p < 1 \times 10^{-6}$).

These findings suggest that central compensation for near-complete cochlear denervation could be supported, in part, through a synergistic increase in AMPA receptor availability (i.e., sensitization) and reduction in $GABA_A$ receptor availability (i.e., disinhibition). Together, sensitization and disinhibition would cooperatively tip the excitatory/inhibitory (E/I) balance in the central pathway toward hyperexcitability. We computed a composite excitation/inhibition (E/I) index in each cell according to the formula (*Gria2* − *Gabra1*)/(*Gria2* + *Gabra1*), where again a value of 0 indicates a balanced transcription of both genes, while positive and negative values indicate transcriptional changes consistent with hyper- or hypo-excitability, respectively. As expected from the results above, E/I indices were significantly more positive in both the ACtx (Fig. 5A) and IC (Fig. 5B) of ouabain-treated mice than vehicle-treated mice (Wilcoxon's rank sum test, $p < 1 \times 10^{-6}$ for both).

We sought to determine whether a consistent relationship existed between the degree of auditory nerve damage and the degree of rebalancing toward a more positive E/I index. We compared ABR Wave 1b amplitudes to the distribution of E/I indices from IC and ACtx in each ouabain-treated mouse (Fig. 5A–C, right, rank-ordered by cortical E/I index) but did not find any obvious relationship between the extent of peripheral neuropathy and the extent of transcriptional E/I balance in the IC or ACtx. For example, the ouabain-treated mice with the strongest and weakest ABR wave 1 amplitudes (O3 and O4 respectively) showed the least pronounced E/I shifts in ACtx and middling E/I shifts in the IC. Although the sample size here is too limited to make any strong conclusions, this confirms prior observations that the extent of compensatory plasticity is not strictly determined by the status of the sensory periphery, and instead may be more directly regulated by local circuit dynamics (Chambers et al., 2016b,a; Resnik and Polley, 2017).

Please cite this article in press as: Balaram P et al. Synergistic Transcriptional Changes in AMPA and $GABA_A$ Receptor Genes Support Compensatory Plasticity Following Unilateral Hearing Loss. Neuroscience (2018), https://doi.org/10.1016/j.neuroscience.2018.08.023

No synergistic shifts in AMPA and GABAA mRNA transcription levels following a shorter period of unilateral auditory deprivation

Neural recovery of sound processing following widespread but selective cochlear afferent loss takes at least one week to emerge and several weeks to reach maximum levels of compensation (Qiu et al., 2000; Chambers et al., 2016a; Resnik and Polley, 2017). Transcriptional changes that underlie homeostatic plasticity processes such as synaptic scaling are generally much faster, ramping up within hours following activity perturbations (Ibata et al., 2008). To assess whether opposing changes in *Gria2* and *Gabra1* mRNA levels following cochlear deafferentation could be an early marker of compensatory plasticity that would appear before physiological indices of excess central gain, we performed a follow-up study that measured transcriptional changes 5 days following unilateral cochlear deafferentation. We chose not to use ouabain for short-term analyses because the degree of cochlear afferent neuropathy is a moving target that steadily increases throughout the first few weeks (Yuan et al., 2013).

To avoid the complications of interpreting transcriptional changes when cochlear afferent loss is not yet complete, we instead used a protocol that induced a more immediate unilateral sensorineural and conductive hearing loss. Immediate short-term unilateral deafness (STUD) was accomplished by removing the tympanic membrane and ossicles in the left ear, puncturing the cochlear oval window, infusing sterile water into the cochlea through the oval window and packing the middle ear space with an absorbent material to wick out cochlear fluids by capillary action (Fig. 6A). Stability of STUD was assessed by measuring cochlear functions 5 days later with the wick removed and the middle ear free of all fluid. When compared to control measurements, we observed that ABR thresholds in the STUD ear were elevated to or above the highest sound level tested (Fig. 6B), ABR wave 1 growth functions were flat (Fig. 6C) and DPOAE thresholds were not measurable at any frequency or level tested (Fig. 6D).

Gabra1 and *Gria2* mRNA levels were quantified in individual neurons from the right ACtx 5 days after STUD (n = 13,282 from STUD and n = 19,862 from controls; Fig. 7A). We observed that *Gabra1* levels were significantly reduced in STUD mice compared to controls (20.27 ± 0.17 vs. 37.2 ± 0.2, mean ± SEM for STUD and vehicle, respectively, unpaired t-test, $p < 1 \times 10^{-6}$), but *Gria2* levels were also significantly lower (31.4 ± 0.23 vs. 58.9 ± 0.25, mean ± SEM for STUD and vehicle, respectively, unpaired t-test, $p < 1 \times 10^{-6}$; Fig. 7B). The reduction in *Gabra1* and *Gria2* transcription levels was approximately equivalent, leading to no clear change in the E/I index in STUD neurons compared to control (0.33 ± 0.58 vs. 0.30 ± 0.37, median ± IQR for STUD and vehicle, respectively; Fig. 7C).

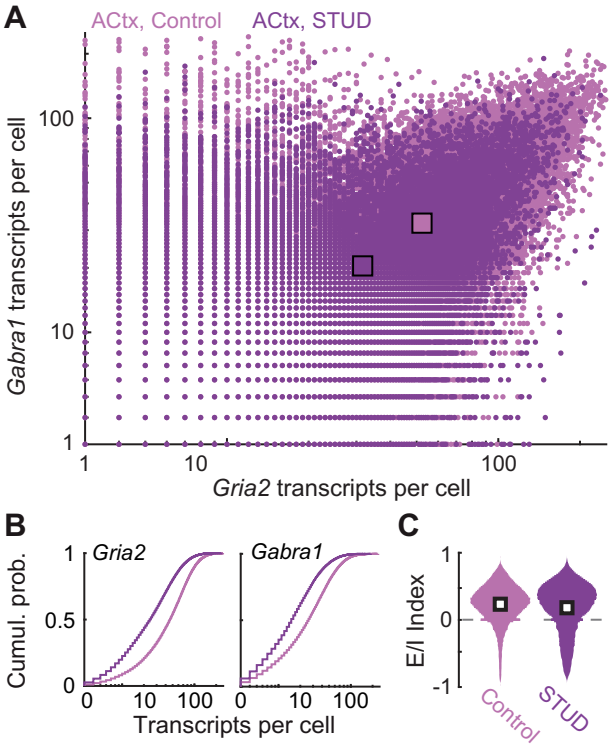

Fig. 7. Equivalent reduction in *Gabra1* and *Gria2* mRNA transcripts produce no net shift in excitatory–inhibitory balance following short-term unilateral deafness. (A) Counts of *Gria2* and *Gabra1* transcripts in the ACtx contralateral to the deafened ear (dark purple hue) or in control mice (light purple hue). Each point represents the number of transcripts for a given cell. Squares indicate means of the *Gria2* and *Gabra1* distributions for each treatment group. (B) Cumulative distributions of *Gria2* and *Gabra1* transcripts in STUD and control mice. (C) The distribution of excitation/inhibition (E/I) index values from all cells in ACtx, according to the formula (*Gria2* – *Gabra1*)/(*Gria2* + *Gabra1*), where zero (dashed gray line) indicates an equivalent number of excitatory (*Gria2*) and inhibitory (*Gabra1*) transcripts. White squares represent the median of each distribution.

Downregulation of AMPA and GABAA mRNA transcription after STUD in genotyped excitatory and inhibitory neurons

We questioned whether a cell type-specific mRNA analysis might reveal more subtle transcriptional rebalancing that was differentially expressed in excitatory and inhibitory neurons (Sturm et al., 2017). For example, excitatory neurons might predominantly express the decrease in *Gabra1* (i.e., disinhibition), whereas inhibitory neurons could dominate the decreased expression of *Gria2* (i.e., sensitization). This would produce a transcriptional rebalancing toward network hyperexcitability that could not be appreciated if all cell types were pooled together in a single analysis. We addressed this possibility by performing the same analysis of *Gria2* and *Gabra1* mRNA, in ACtx neurons that were genotyped as either excitatory or inhibitory, depending on whether they expressed vesicular glutamate transporter 1 (*VGLUT1*) or vesicular GABA transporter (*VGAT*) mRNA, respectively (Fig. 8A-B). Contrary to our prediction, we found that the commensurate downward regulation of both transcripts at the level of the population (Fig. 7)

Please cite this article in press as: Balaram P et al. Synergistic Transcriptional Changes in AMPA and GABA$_A$ Receptor Genes Support Compensatory Plasticity Following Unilateral Hearing Loss. Neuroscience (2018), https://doi.org/10.1016/j.neuroscience.2018.08.023

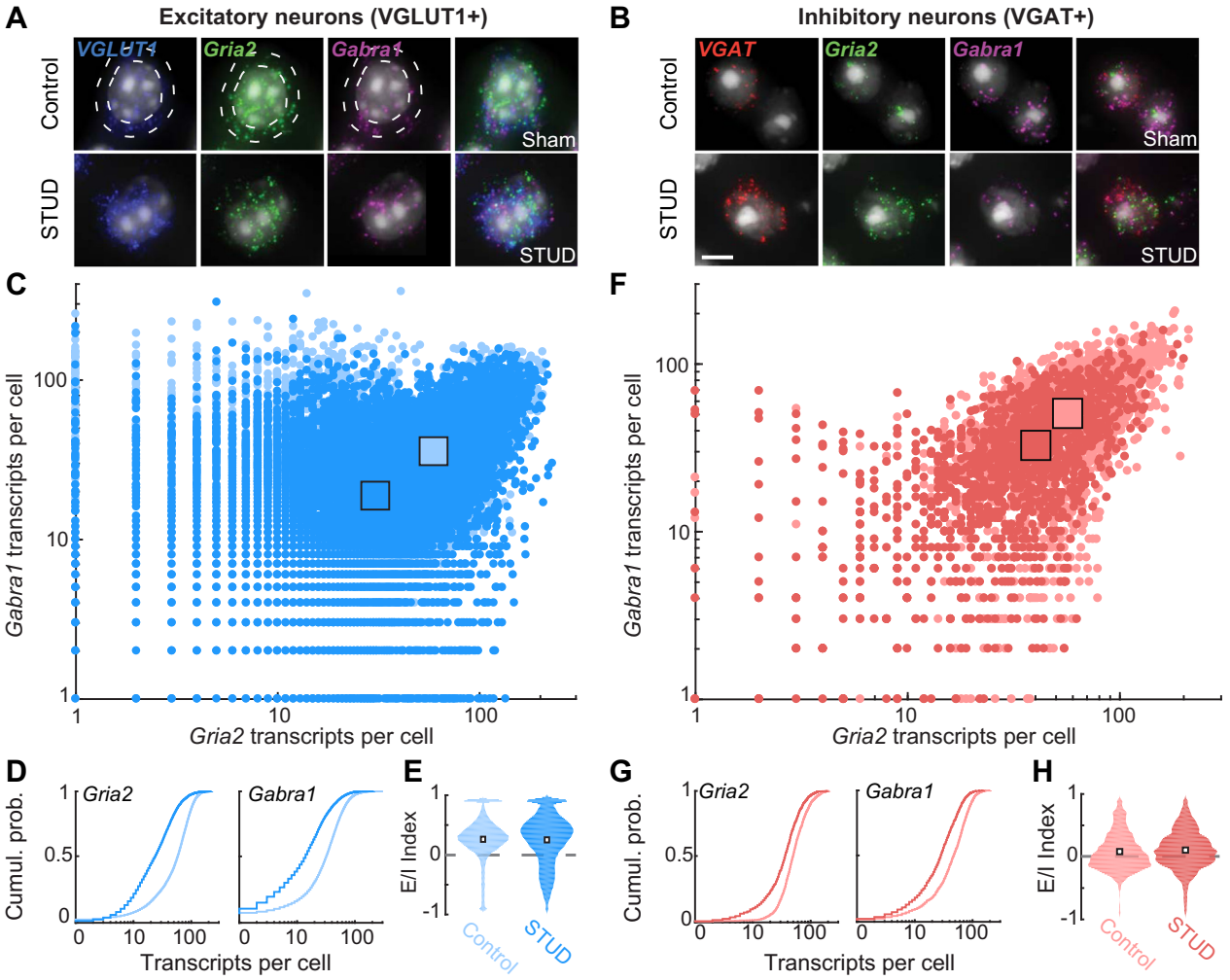

Fig. 8. Parallel reductions in *Gabra1* and *Gria2* mRNA levels after STUD are observed both in excitatory and inhibitory ACtx neurons. (A, B) four-channel fluorescence microscopy supports identification of DAPI-labeled nuclei (white) alongside mRNA transcripts for *Gria2* (green), *Gabra1* (magenta) and either the vesicular glutate transporter 1 mRNA (*VGLUT1*, blue, A) or the vesicular GABA transporter (*VGAT*, red, B). The presence of *VGLUT1* or *VGAT* mRNA in the perinuclear region (white circles in *A*) was used to genotype the neuron as excitatory or inhibitory and also to count the number of *Gria2* and *Gabra1* transcripts, as per all prior measurements. Scale bar = 5 μm. (C) Counts of *Gria2* and *Gabra1* transcripts in *VGLUT1* + excitatory neurons in the ACtx contralateral to the deafened ear (dark blue hue) or in control mice (light blue hue). Each point represents the number of transcripts for a given cell. Squares indicate means of the *Gria2* and *Gabra1* distributions for each treatment group. (D) Cumulative distributions of *Gria2* and *Gabra1* transcripts from *VGLUT1* + excitatory neurons in STUD and control mice. (E) The distribution of excitation/inhibition (E/I) index values from all *VGLUT1* + excitatory cells in ACtx, according to the formula (*Gria2* − *Gabra1*)/(*Gria2* + *Gabra1*), where zero (dashed gray line) indicates an equivalent number of excitatory (*Gria2*) and inhibitory (*Gabra1*) transcripts. White squares represent the median of each distribution. (F–H) Same as *C–E*, but for *VGAT* + inhibitory neurons.

was supported by parallel changes in both excitatory neurons (Fig. 8C–E) and inhibitory neurons (Fig. 8F–H). Thus, in contrast to long-term deafferentation following ouabain, we only found evidence for a matched reduction in both *Gria2* and *Gabra1* mRNA in ACtx neurons that produce no net change in the E/I balance in either excitatory or inhibitory ACtx neurons following shorter recovery periods.

DISCUSSION

In this study, we reaffirmed that ouabain application to the cochlear round window membrane eliminates sound-evoked ABRs while largely sparing pre-neural cochlear mechanics (Fig. 1). We demonstrated that individual cells in the IC and ACtx increase *Gria2* expression and decrease *Gabra1* expression after 30 days of unilateral cochlear deafferentation (Figs. 2 and 3). Both elevations in *Gria2* levels and reductions in *Gabra1* levels were more pronounced in the ACtx compared to the IC (Fig. 4) but are not directly correlated with the extent of peripheral cochlear neuropathy (Fig. 5). Synergistic shifts in *Gria2* and *Gabra1* expression were not observed following a shorter recovery period from unilateral hearing loss, where transcription levels of both genes were reduced (Figs. 6–8).

Direct comparisons between the ouabain-based long-term deprivation and the short-term deprivation with STUD should be interpreted cautiously in light of procedural differences between the two experiments.

Please cite this article in press as: Balaram P et al. Synergistic Transcriptional Changes in AMPA and $GABA_A$ Receptor Genes Support Compensatory Plasticity Following Unilateral Hearing Loss. Neuroscience (2018), https://doi.org/10.1016/j.neuroscience.2018.08.023

For instance, different mouse strains were used for each method of hearing loss studies to say nothing of significant differences in the degree and form of unilateral hearing loss between the two approaches. Given that hearing loss was more complete with cochlear water infusion, this difference would have biased us toward finding a greater degree of compensatory changes following STUD compared with ouabain, not less. Instead, the findings reported here match prior physiological characterizations of central auditory recovery following cochlear afferent denervation, where enhanced central gain was more robust one month after afferent damage than one week and is also more pronounced in the thalamus and cortex than in the midbrain (Qiu et al., 2000; Chambers et al., 2016a,b; Resnik and Polley, 2017).

Complementary changes in AMPA and GABAA subunit transcription within individual cells could reflect homeostatic plasticity mechanisms that scale postsynaptic receptor distributions in response to changes in afferent drive (Turrigiano, 2011). Activity perturbations in cultured neurons demonstrate that elevated *Gria2* expression and subsequent AMPA receptor accumulation are critical steps in upward scaling of excitatory synaptic strength (O'Brien et al., 1998; Wierenga et al., 2005; Gainey et al., 2009; Lambo and Turrigiano, 2013), while reductions in $GABA_A$ receptor distributions lead to decreases in inhibitory synaptic strength (Kilman et al., 2002). Removing peripheral visual or somatosensory input *in vivo* can lead to opposing shifts in AMPA and $GABA_A$ receptor densities across cortical brain regions, which presumably contribute to cortical reorganization and the recovery of sensory-evoked activity (Garraghty et al., 2006; He et al., 2006; Mowery et al., 2013). In the auditory system, homeostatic mechanisms may support rebalanced excitation and inhibition in the IC and ACtx after developmental or adult hearing loss (Kotak et al., 2005; Yang et al., 2011; Sturm et al., 2017; Teichert et al., 2017) and altered distributions of AMPA and $GABA_A$ receptors have been reported to accompany cochlear trauma (Suneja et al., 2000; Holt et al., 2005; Dong et al., 2010a,b; Browne et al., 2012).

The findings reported here identified two transcriptional changes that may underlie enhanced central gain following sudden hearing loss, but are by no means a complete description of the full set of changes. Acute hearing loss in adulthood shifts the mRNA and protein expression of multiple AMPA and GABAA receptor subunits, as well as other receptor types (Suneja et al., 1998, 2000; Milbrandt et al., 2000; Holt et al., 2005; Argence et al., 2006; Dong et al., 2010a; Smith et al., 2014) in addition to changes in voltage-gated channels that regulate intrinsic excitability (Yang et al., 2012; Li et al., 2015). Central gain-related changes in postsynaptic receptor densities are likely to vary by neuronal type, such that activity levels across some neural types are stable or suppressed, while others may become increasingly excitable (Takesian et al., 2013; Anderson et al., 2017; Sturm et al., 2017). Here, we used VGLUT and VGAT mRNA to coarsely group neurons into excitatory and inhibitory sub-classes (Fig. 8), though we did not observe differences between these genetic categories in the STUD condition. A deeper analysis of cell-type specific shifts in *Gria2* and *Gabra1* expression, alongside the expression patterns of other subunits or receptor types, may elucidate the intracellular mechanisms that drive neuronal hyperactivity after peripheral deafferentation. A more comprehensive understanding of such mechanisms can potentially identify therapeutic targets for debilitating perceptual disorders such as tinnitus, hyperacusis, phantom limb pain, or visual release hallucinations.

ACKNOWLEDGMENTS

This work was supported by grants and fellowships from the National Institute of Deafness and Other Communication Disorders (DC009836 (DP), DC015388 (TH) and DC015710 (PB) as well as a research grant from Autifony Therapeutics (DP) and other financial support from the Lauer Tinnitus Research Center (DP). TAH developed initial RNAscope protocols. All authors contributed to experimental design. PB collected and analyzed the data. PB and DP wrote the manuscript. We thank J. L'Heureux and B. Robert for their help developing Matlab scripts for mRNA quantification.

REFERENCES

Anderson CT, Kumar M, Xiong S, Tzounopoulos T (2017) Cell-specific gain modulation by synaptically released zinc in cortical circuits of audition. eLife 6:1–20.

Argence M, Saez I, Sassu R, Vassias I, Vidal PP, de Waele C (2006) Modulation of inhibitory and excitatory synaptic transmission in rat inferior colliculus after unilateral cochleectomy: an in situ and immunofluorescence study. Neuroscience 141:1193–1207.

Asokan MM, Williamson RS, Hancock KE, Polley DB (2018) Sensory overamplification in layer 5 auditory corticofugal projection neurons following cochlear nerve synaptic damage. Nat Commun:9.

Auerbach BD, Rodrigues PV, Salvi RJ (2014) Central gain control in tinnitus and hyperacusis. Front Neurol. 24(5):206.

Browne CJ, Morley JW, Parsons CH (2012) Tracking the expression of excitatory and inhibitory neurotransmission-related proteins and neuroplasticity markers after noise induced hearing loss Gilestro GF, ed. PLoS One 7 e33272.

Buran BN, Strenzke N, Neef A, Gundelfinger ED, Moser T, Liberman MC (2010) Onset coding Is degraded in auditory nerve fibers from mutant mice lacking synaptic ribbons. J Neurosci 30:7587–7597.

Cai R, Zhou X, Guo F, Xu J, Zhang J, Sun X (2010) Maintenance of enriched environment-induced changes of auditory spatial sensitivity and expression of GABAA, NMDA, and AMPA receptor subunits in rat auditory cortex. Neurobiol Learn Mem 94:452–460.

Caicedo A, Eybalin M (1999) Glutamate receptor phenotypes in the auditory brainstem and mid-brain of the developing rat. Eur J Neurosci 11:51–74.

Caspary DM, Hughes LF, Ling LL (2013) Age-related GABAA receptor changes in rat auditory cortex. Neurobiol Aging 34:1486–1496.

Caspary DM, Milbrandt JC, Helfert RH (1995) Central auditory aging: GABA changes in the inferior colliculus. Exp Gerontol 30:349–360.

Chambers AR, Resnik J, Yuan Y, Whitton JP, Edge AS, Liberman MC, Polley DB (2016a) Central gain restores auditory processing following near-complete cochlear denervation. Neuron 89:1–13.

Chambers AR, Salazar JJ, Polley DB (2016b) Persistent thalamic sound processing despite profound cochlear denervation. Front Neural Circuits 10:1–13.

Dong S, Mulders WHAM, Rodger J, Robertson D (2009) Changes in neuronal activity and gene expression in guinea-pig auditory brainstem after unilateral partial hearing loss. Neuroscience 159:1164–1174.

Dong S, Mulders WHAM, Rodger J, Woo S, Robertson D (2010a) Acoustic trauma evokes hyperactivity and changes in gene expression in guinea-pig auditory brainstem. Eur J Neurosci 31:1616–1628.

Dong S, Rodger J, Mulders WHAM, Robertson D (2010b) Tonotopic changes in GABA receptor expression in guinea pig inferior colliculus after partial unilateral hearing loss. Brain Res 1342:24–32.

Gainey MA, Hurvitz-Wolff JR, Lambo ME, Turrigiano GG (2009) Synaptic scaling requires the GluR2 subunit of the AMPA receptor. J Neurosci 29:6479–6489.

Galbraith G, Waschek J, Armstrong B, Edmond J, Lopez I, Liu W, Kurtz I (2006) Murine auditory brainstem evoked response: putative two-channel differentiation of peripheral and central neural pathways. J Neurosci Methods 153:214–220.

Garraghty PE, Arnold LL, Wellman CL, Mowery TM (2006) Receptor autoradiographic correlates of deafferentation-induced reorganization in adult primate somatosensory cortex. J Comp Neurol 497:636–645.

Gutiérrez A, Khan ZU, Morris SJ, De Blas AL (1994) Age-related decrease of GABAA receptor subunits and glutamic acid decarboxylase in the rat inferior colliculus. J Neurosci 14:7469–7477.

Hackett TA, Clause AR, Takahata T, Hackett NJ, Polley DB (2015) Differential maturation of vesicular glutamate and GABA transporter expression in the mouse auditory forebrain during the first weeks of hearing. Brain Struct Funct 221:2619–2673.

Hackett TA, Rinaldi Barkat T, O'Brien BMJ, Hensch TK, Polley DB (2011) Linking topography to tonotopy in the mouse auditory thalamocortical circuit. J Neurosci 31:2983–2995.

He H-Y, Hodos W, Quinlan EM (2006) Visual deprivation reactivates rapid ocular dominance plasticity in adult visual cortex. J Neurosci 26:2951–2955.

Holt AG, Asako M, Lomax CA, MacDonald JW, Tong L, Lomax MI, Altschuler RA (2005) Deafness-related plasticity in the inferior colliculus: gene expression profiling following removal of peripheral activity. J Neurochem 93:1069–1086.

Humanes-Valera D, Foffani G, Alonso-Calviño E, Fernández-López E, Aguilar J (2017) Dual cortical plasticity after spinal cord injury. Cereb Cortex 27:2926–2940.

Ibata K, Sun Q, Turrigiano GG (2008) Rapid synaptic scaling induced by changes in postsynaptic firing. Neuron 57:819–826.

Jaepel J, Hübener M, Bonhoeffer T, Rose T (2017) Lateral geniculate neurons projecting to primary visual cortex show ocular dominance plasticity in adult mice. Nat Neurosci 20:1708–1714.

Jiang C, Luo B, Manohar S, Chen G-D, Salvi R (2017) Plastic changes along auditory pathway during salicylate-induced ototoxicity: hyperactivity and CF shifts. Hear Res 347:28–40.

Jones EG, Pons TP (1998) Thalamic and brainstem contributions to large-scale plasticity of primate somatosensory cortex. Science 282:1121–1125.

Kaas JH, Krubitzer LA, Chino YM, Langston AL, Polley EH, Blair N (1990) Reorganization of retinotopic cortical maps in adult mammals after lesions of the retina. Science 248:229–231.

Kamke MR, Brown M, Irvine DRF (2003) Plasticity in the tonotopic organization of the medial geniculate body in adult cats following restricted unilateral cochlear lesions. J Comp Neurol 459:355–367.

Kilman V, van Rossum MCW, Turrigiano GG (2002) Activity deprivation reduces miniature IPSC amplitude by decreasing the number of postsynaptic GABA(A) receptors clustered at neocortical synapses. J Neurosci Neur 22:1328–1337.

Kotak VC, Fujisawa S, Lee FA, Karthikeyan O, Aoki C, Sanes DH (2005) Hearing loss raises excitability in the auditory cortex. J Neurosci 25:3908–3918.

Kotak VC, Korada S, Schwartz IR, Sanes DH (1998) A developmental shift from GABAergic to glycinergic transmission in the central auditory system. J Neurosci 18:4646–4655.

Lambo ME, Turrigiano GG (2013) Synaptic and intrinsic homeostatic mechanisms cooperate to increase L2/3 pyramidal neuron excitability during a late phase of critical period plasticity. J Neurosci 33:8810–8819.

Lang H, Schulte BA, Schmiedt RA (2005) Ouabain induces apoptotic cell death in Type I spiral ganglion neurons, but not Type II neurons. J Assoc Res Otolaryngol 6:63–74.

Li S, Kalappa BI, Tzounopoulos T (2015) Noise-induced plasticity of KCNQ2/3 and HCN channels underlies vulnerability and resilience to tinnitus. eLife 4:1–23.

Lobarinas E, Salvi R, Ding D (2013) Insensitivity of the audiogram to carboplatin induced inner hair cell loss in chinchillas. Hear Res:1–8.

Marsden KC, Beattie JB, Friedenthal J, Carroll RC (2007) Cellular/molecular NMDA receptor activation potentiates inhibitory transmission through GABA receptor-associated protein- dependent exocytosis of GABA A Receptors. J Neurosci 27:14326–14337.

Melcher JR, Guinan JJ, Knudson IM, Kiang NYS (1996) Generators of the brainstem auditory evoked potential in cat. II. Correlating lesion sites with waveform changes. Hear Res 93:28–51.

Merzenich MM, Kaas J, Wall J, Nelson RJ, Sur M, Felleman D, Nelson RJ, Sur M, Felleman D (1983) Topographic reorganization of somatosensory cortical areas 3B and 1 in adult monkeys following restricted deafferentation. Neuroscience 8:33–55.

Milbrandt JC, Albin RL, Caspary DM (1994) Age-related decrease in GABAB receptor binding in the Fischer 344 rat inferior colliculus. Neurobiol Aging 15:699–703.

Milbrandt JC, Holder TM, Wilson MC, Salvi RJ, Caspary DM (2000) GAD levels and muscimol binding in rat inferior colliculus following acoustic trauma. Hear Res 147:251–260.

Milbrandt JC, Hunter C, Caspary DM (1997) Alterations of GABA A receptor subunit mRNA levels in the aging Fischer 344 rat inferior colliculus. J Comp Neurol 379:455–465.

Mowery TM, Walls SM, Garraghty PE (2013) AMPA and GABAA/B receptor subunit expression in the cortex of adult squirrel monkeys during peripheral nerve regeneration. Brain Res 1520:80–94.

Mowery TM, Kotak VC, Sanes DH (2015) Transient hearing loss within a critical period causes persistent changes to cellular properties in adult auditory cortex. Cereb Cortex. 25 (8):2083–2094.

O'Brien RJ, Kamboj S, Ehlers MD, Rosen KR, Fischbach GD, Huganir RL (1998) Activity-dependent modulation of synaptic AMPA receptor accumulation. Neuron 21:1067–1078.

Petrus E, Rodriguez G, Patterson R, Connor B, Kanold PO, Lee H-K (2015) Vision loss shifts the balance of feedforward and intracortical circuits in opposite directions in mouse primary auditory and visual cortices. J Neurosci 35:8790–8801.

Qiu C, Salvi R, Ding D, Burkard R (2000) Inner hair cell loss leads to enhanced response amplitudes in auditory cortex of unanesthetized chinchillas: evidence for increased system gain. Hear Res 139:153–171.

Raza A, Milbrandt JC, Arneric SP, Caspary DM (1994) Age-related changes in brainstem auditory neurotransmitters: measures of GABA and acetylcholine function. Hear Res 77:221–230.

Resnik JDB (2017) Polley Fast-spiking GABA circuit dynamics in the auditory cortex predict recovery of sensory processing following peripheral nerve damage. eLife 6.

Robertson D, Irvine DRF (1989) Plasticity of frequency organization in auditory cortex of guinea pigs with partial unilateral deafness. J Comp Neurol 282:456–471.

Sanes DH, Kotak VC (2011) Developmental plasticity of auditory cortical inhibitory synapses. Hear Res 279:140–148.

Please cite this article in press as: Balaram P et al. Synergistic Transcriptional Changes in AMPA and $GABA_A$ Receptor Genes Support Compensatory Plasticity Following Unilateral Hearing Loss. Neuroscience (2018), https://doi.org/10.1016/j.neuroscience.2018.08.023

Schuknecht HF, Woellner RC (1953) Hearing losses following partial section of the cochlear nerve. Laryngoscope 63:441–465.

Shim HJ, Lee LH, Huh Y, Lee SY, Yeo SG (2012) Age-related changes in the expression of NMDA, serotonin, and GAD in the central auditory system of the rat. Acta Otolaryngol 132:44–50.

Smith AR, Kwon JH, Navarro M, Hurley LM (2014) Acoustic trauma triggers upregulation of serotonin receptor genes. Hear Res 315:40–48.

Sturm JJ, Zhang-Hooks Y-X, Roos H, Nguyen T, Kandler K (2017) Noise trauma induced behavioral gap detection deficits correlate with reorganization of excitatory and inhibitory local circuits in the inferior colliculus and are prevented by acoustic enrichment. J Neurosci 37:0602–0617.

Sun W, Mercado E, Wang P, Shan X, Lee T-C, Salvi RJ (2005) Changes in NMDA receptor expression in auditory cortex after learning. Neurosci Lett 374:63–68.

Suneja SK, Benson CG, Potashner SJ (1998) Glycine receptors in adult guinea pig brain stem auditory nuclei: regulation after unilateral cochlear ablation. Exp Neurol 154:473–488.

Suneja SKK, Potashner SJJ, Benson CGG (2000) AMPA receptor binding in adult guinea pig brain stem auditory nuclei after unilateral cochlear ablation. Exp Neurol 165:355–369.

Takesian AE, Kotak VC, Sharma N, Sanes DH (2013) Hearing loss differentially affects thalamic drive to two cortical interneuron subtypes. J Neurophysiol 110:999–1008.

Teichert M, Liebmann L, Hübner CA, Bolz J (2017) Homeostatic plasticity and synaptic scaling in the adult mouse auditory cortex. Sci Rep 7:17423.

Turrigiano G (2011) Too many cooks? Intrinsic and synaptic homeostatic mechanisms in cortical circuit refinement. Annu Rev Neurosci 34:89–103.

Turrigiano GG, Leslie KR, Desai NS, Rutherford LC, Nelson SB (1998) Activity-dependent scaling of quantal amplitude in neocortical neurons. Nature 391:892–896.

Wang F, Flanagan J, Su N, Wang LC, Bui S, Nielson A, Wu X, Vo HT, Ma XJ, Luo Y (2012) RNAscope: a novel in situ RNA analysis platform for formalin-fixed, paraffin-embedded tissues. J Mol Diagnostics 14:22–29.

Wang J, Ding D, Salvi RJ (2002) Functional reorganization in chinchilla inferior colliculus associated with chronic and acute cochlear damage. Hear Res 168:238–249.

Wang Z, Ruan Q, Wang D (2005) Different effects of intracochlear sensory and neuronal injury stimulation on expression of synaptic N-methyl-D-aspartate receptors in the auditory cortex of rats in vivo. Acta Otolaryngol 125:1145–1151.

Wekselblatt JB, Flister ED, Piscopo DM, Niell CM (2016) Large-scale imaging of cortical dynamics during sensory perception and behavior. J Neurophysiol 115:2852–2866.

Wierenga CJ, Ibata K, Turrigiano GG (2005) Postsynaptic expression of homeostatic plasticity at neocortical synapses. J Neurosci 25:2895–2905.

Wong-Riley MT, Jacobs P (2002) AMPA glutamate receptor subunit 2 in normal and visually deprived macaque visual cortex. Vis Neurosci. 19(5):563–573.

Yang S, Su W, Bao S (2012) Long-term, but not transient, threshold shifts alter the morphology and increase the excitability of cortical pyramidal neurons. J Neurophysiol 108:1567–1574.

Yang S, Weiner BD, Zhang LS, Cho S-JS-J, Bao S (2011) Homeostatic plasticity drives tinnitus perception in an animal model. Proc Natl Acad Sci 108:14974–14979.

Yu ZY, Wang W, Fritschy JM, Witte OW, Redecker C (2006) Changes in neocortical and hippocampal GABAA receptor subunit distribution during brain maturation and aging. Brain Res 1099:73–81.

Yuan Y, Shi F, Yin Y, Tong M, Lang H, Polley DB, Liberman MC, Edge ASB (2013) Ouabain-induced cochlear nerve degeneration: synaptic loss and plasticity in a mouse model of auditory neuropathy. J Assoc Res Otolaryngol 15:31–43.

Zeng FG (2005) Perceptual consequences of disrupted auditory nerve activity. J Neurophysiol 93:3050–3063.

Zhang Y, Cudmore RH, Lin D-T, Linden DJ, Huganir RL (2015) Visualization of NMDA receptor-dependent AMPA receptor synaptic plasticity in vivo. Nat Neurosci 18.

(Received 20 June 2018, Accepted 22 August 2018)
(Available online xxxx)